CHINESE OPTICS LETTERS

Vol. 20, No. 3 | March 2022

Wavelength-tunable barium gallate persistent luminescence phosphors with enhanced luminescence

Qianting Yang (杨倩婷), Renagul Abdurahman (热娜古丽·阿不都热合曼)*, Tongsheng Yang (杨通胜), and Xuefeng Sun (孙雪峰)

Xinjiang Laboratory of Native Medicinal and Edible Plant Resources Chemistry, College of Chemistry and Environmental Sciences, Kashi University, Kashi 844007, China

*Corresponding author: renagul111@aliyun.com

Received November 18, 2021 | Accepted December 29, 2021 | Posted Online January 26, 2022

The near-infrared (NIR) emitting wavelength-tunable Cr^{3+}-doped barium gallate (BGO:Cr) persistent luminescence (PersL) phosphors with enhanced luminescence were reported. The emission wavelength of the BGO:Cr PersL phosphors was adjusted from 715 to 739 nm by varying the amount of Cr^{3+} and the ratio of Ga:Ba. Meanwhile, the luminescence intensity and afterglow of the BGO:Cr PersL phosphors were enhanced. BGO:Cr PersL phosphors exhibited UV excitation, LED light restimulation, PersL for more than 6 days, and excellent capability for information storage, which was expected to promote the development of cheap and wavelength-tunable PersL materials for practical applications.

Keywords: persistent luminescence; Cr^{3+} doping; barium gallate.
DOI: 10.3788/COL202220.031602

1. Introduction

Persistent luminescence (PersL) phosphors own an interesting phenomenon where luminescence lasts for hours, even a few days, after the cessation of excitation[1]. Such phosphors attracted considerable attention, which are widely used in the fields of emergency command, information storage, and biological imaging[2,3]. In particular, the near-infrared (NIR) emitting PersL phosphors comprise some unique features of high signal-to-noise ratios (SNRs) and wide excitation spectral regions, which attracted much attention toward their application in the next-generation high-capacity storage systems. The input information was recorded into the PersL phosphors by capturing the incident photons at energy traps to complete the information storage, and the output signal was retrieved by releasing the trapped charge carriers and emitting the photons[3]. The multi-spectral excited NIR PersL phosphor ($Zn_{1.25}Ga_{1.5}Ge_{0.25}O_4:Cr^{3+}$) with a high quantum efficiency was reported and employed as a promising storage medium for optical information storage and readout[4]. Zhan *et al.* developed a novel NIR PersL phosphor ($Mg_4Ga_4Ge_3O_{16}:Cr^{3+}$) for optical information recording, which had the characteristics of write-in, read-out, and renewable information storage[5]. However, these NIR emitting PersL phosphors are with high cost.

For the NIR PersL phosphors, Eu^{2+}-doped sulfides such as $CaS:Eu^{2+}$, $SrS:Eu^{2+}$ and Eu^{3+}-doped sulfides such as $Y_2O_2S:Eu^{3+}$, Mg^{2+}, Ti^{4+} are well known[6]. However, the sulfurization agent is harmful to environment. Meanwhile, it is common to obtain green/blue PersL in Eu^{2+}-doped oxide hosts, and it is difficult to find suitable oxide hosts for Eu^{2+} in order to obtain red PersL[7]. Barium gallate ($BaGa_2O_4$, BGO) with double oxides composition exhibits tetrahedral framework topology and exists in a variety of polymorphs, which is a promising membrane without expensive rare-earth ions assisted luminescence[8]. Additionally, the activation energy of the electrons in the BGO trap centers is 0.61 ± 0.01 eV [9], which was interrelated with the PersL intensity and durations of the PersL phosphors, aiming to retain the recorded information for a long time[10]. Li's group developed a Bi^{3+}-doped orange emitting and naked-eye observable BGO phosphor with commendable PersL[11]. Zhou *et al.* reported Sm^{3+}-doped 656 nm emitting BGO PersL phosphors via a high-temperature solid-state method[12]. However, the phosphors still suffer from limited penetration depth.

The Cr^{3+}-doped NIR emitting PersL phosphors with the emission range of 650–1000 nm were renewable by red light instead of UV light, which is highly promising for efficient optical storage and renewable tissue imaging *in vivo*. There were many reports on Cr^{3+}-doped gallates, such as $ZnGa_2O_4:Cr^{3+}$[13], $Zn_3Ga_2GeO_8:Cr^{3+}$[14], $LiGa_5O_8:Cr^{3+}$[15], and $MgGa_2O_4:Cr^{3+}$ [16], which had the disadvantages of high cost and non-adjustable emission wavelength. The wavelength-tunable PersL phosphors provide superior performance in optoelectronic applications, such as information carriers for high-density encrypted data storage, anti-counterfeiting, and

multiplexed bioassay[17,18]. The wavelength-tunable phosphors can be applied to UV chips and in phosphor-converting NIR-LED devices[19]. Therefore, it is of great significance to develop new NIR emitting PersL phosphors based on the BGO host with low cost and tunable wavelength. Considering the excellent properties of the BGO host and Cr^{3+} in the PersL phosphors, the introduction of Cr^{3+} into the BGO host is the potential to achieve more unique NIR emission PersL phosphors.

Herein, a wavelength-tunable BGO:Cr PersL phosphor was firstly developed by the solid-state synthesis method. The luminescence of BGO was transformed from a wide blue emission to an NIR emission after doping Cr. The emission wavelengths and luminescence intensity of the BGO:Cr PersL phosphors were adjusted by varying the doping amount of Cr^{3+} and the ratio of Ga:Ba. The prepared BGO:Cr PersL phosphors exhibited UV excitation, LED light repeated excitation, stable phase, PersL for more than 6 days, and excellent capability for information storage.

2. Experiments

The experiment section is provided in Supplementary Materials.

3. Experimental Results and Analysis

3.1. Influence of Cr^{3+} ions and Ba^{2+} ions on the optical property in $BaGa_2O_4$

Figure 1 shows the emission spectra of the $BaGa_2O_4:Cr_x$ ($x = 0$, 0.006, 0.02, 0.04, 0.06, 0.08, and 0.10) PersL phosphors. Under the excitation at 254 nm of the UV lamp, the BGO host exhibited a broad blue emission in the range of 300–600 nm with the maximum emission wavelength at 450 nm, which was due to the native defects originated from the octahedral GaO_6 unit in the BGO host[9]. The emission of the BGO host disappeared after doping various amounts of Cr^{3+} ($x = 0.006$–0.10), and the emission peaks at 715–731 nm were generated (Fig. 1, Table S1 in Supplementary Materials), which were produced by the spin-forbidden $^2E(^2G) \rightarrow {}^4A_2(^4F)$ transition of Cr^{3+}[20]. Especially, $BaGa_2O_4:Cr_x$ showed a peak at 715 nm when $x = 0.006$, and the red shift occurred at 727 nm when $x = 0.04$; then the peak red-shifted to 731 nm when $x = 0.06$, which was ascribed to the decrease of the crystal-field intensity at the Cr^{3+} center caused by the increase of Cr^{3+}[21]. Among them, $BaGa_2O_4:Cr_{0.06}$ showed the highest photoluminescence (PL) intensity with the optimal number of luminescence centers, and the PL intensity decreased when the concentration (x value) raised over 0.06, which was called concentration quenching caused by the decrease of the Cr-Cr distance. The non-radioactive energy migration within the doping ions was activated when the Cr-Cr distance decreased[22]. Compared with the $BaGa_2O_4$ matrix, the PersL performance of the $BaGa_2O_4:Cr_{0.06}$ was significantly optimized by replacing Ga^{3+} (Fig. 2, Fig. S1 in Supplementary Materials) with the luminescent center Cr^{3+} in the matrix[23].

The optical properties of Cr^{3+} ions on the octahedra are known strongly depending on the crystal-field environment. To evaluate the luminescence properties of BGO:Cr^{3+}, the crystal-field parameter (D_q) and the Racah parameter B can be calculated by the following equations[24]:

$$10D_q = \nu_2, \tag{1}$$

$$B = \frac{\nu_1^2 + 2\nu_2^2 - 3\nu_1\nu_2}{15\nu_1 - 27\nu_2}. \tag{2}$$

Here, ν_1 and ν_2 correspond to the peak energies of the excitation bands $^4A_2(^4F) \rightarrow {}^4T_1(^4F)$ and $^4A_2(^4F) \rightarrow {}^4T_2(^4F)$ transitions, respectively (Fig. S3 in Supplementary Materials). The values of D_q and B are calculated to be about 1953 cm^{-1} and 669 cm^{-1}, respectively. Therefore, the value of D_q/B is estimated to be ~2.919. Figure S4 in Supplementary Materials presents the Tanabe–Sugano energy-level diagram, which demonstrates the optical properties of Cr^{3+} ions on the octahedra. The moderate value of the D_q/B for Cr^{3+} in BGO suggests that broad and narrow emission bands have simultaneous presence, and the narrow emission band $^2E(^2G) \rightarrow {}^4A_2(^4F)$ is the dominant transition[4].

The composition ratio affected the crystal structure and luminescence properties of the PersL phosphors[25]. Therefore, the effects of the Ga/Ba ratio on the luminescent properties of the

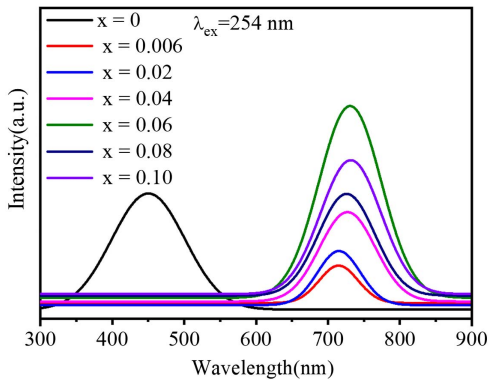

Fig. 1. Emission spectra of $BaGa_2O_4:Cr_x$ (x = 0, 0.006, 0.02, 0.04, 0.06, 0.08, and 0.10) PersL phosphors.

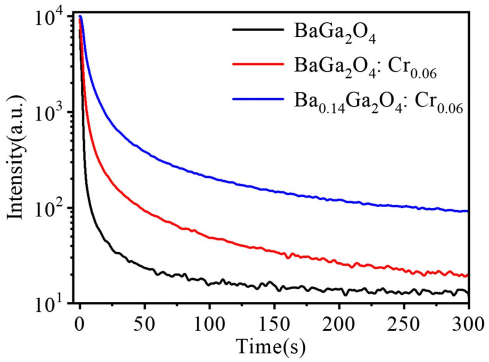

Fig. 2. PersL curves of $BaGa_2O_4$, $BaGa_2O_4:Cr_{0.06}$, and $Ba_{0.14}Ga_2O_4:Cr_{0.06}$ PersL phosphors.

Table 1. Parameters of Afterglow Decay Curve Fitting.

Samples	τ_1/s	A_1	τ_2/s	A_2	τ_3/s	A_3	τ_{av}/s	R^2
$BaGa_2O_4$	3.90	406.06	0.66	12,172.33	31.50	52.53	5.09	0.9997
$BaGa_2O_4:Cr_{0.06}$	4.06	1786.91	15.79	385.69	79.72	112.63	36.37	0.9997
$Ba_{0.14}Ga_2O_4:Cr_{0.06}$	5.92	4722.47	20.66	1105.57	90.89	359.05	41.21	0.9998

BGO:Cr PersL phosphors were investigated by changing the y value (Ba^{2+} ion amount, Ga/Ba ratio) of $Ba_yGa_2O_4:Cr_{0.06}$. Figure S5 in Supplementary Materials shows the emission spectra of the $Ba_yGa_2O_4:Cr_{0.06}$ ($y = 0.08$, 0.10, 0.12, 0.14, 0.16, 0.18, and 1) PersL phosphors excited by 254 nm light. Compared with $BaGa_2O_4:Cr_{0.06}$, the emission peaks have red-shifted to 739 nm, and the intensity of the luminescence was enhanced markedly when the y value was less than 0.18, which was due to the excellent ability of the Cr^{3+} ions to substitute Ga^{3+} ions at the distorted octahedral sites and the suitable host crystal-field strength around Cr^{3+} ions in β-Ga_2O_3 for intense NIR luminescence[26] (Fig. S6 in Supplementary Materials). The intensity of the emission peak reached the maximum value when $y = 0.14$, which benefited from the optimal composition of the sample for luminescence at this time. The PersL intensities of BGO were further enhanced after changing the amount of Cr^{3+} and the ratio of Ga:Ba (Fig. 2, Fig. S1 in Supplementary Materials), which may be caused by the solid-state reaction preparation of β-$Ga_2O_3:Cr^{3+}$, Ba^{2+} particles possessing more defects (traps) for PersL than the $BaGa_2O_4$.

The decay curves can be well fitted to a three-exponential equation, as follows[27]:

$$I(t) = I_0 + A_1 \exp\left(\frac{-t}{\tau_1}\right) + A_2 \exp\left(\frac{-t}{\tau_2}\right) + A_3 \exp\left(\frac{-t}{\tau_3}\right), \quad (3)$$

where $I(t)$ is the luminescence intensity at time t, A_1, A_2, and A_3 are constants, and τ_1, τ_2, and τ_3 are the decay times for the exponential components. The τ_1, τ_2, and τ_3 parameters of the decay curves reflect the three-stage afterglow attenuation with fast attenuation, attenuation, and slow attenuation, respectively. Table 1 shows the fitting parameters, the coefficient of determination (R^2), and the average lifetime (τ_{av}) calculated from the PersL decay curves for $BaGa_2O_4$, $BaGa_2O_4:Cr_{0.06}$, and $Ba_{0.14}Ga_2O_4:Cr_{0.06}$ PersL phosphors. The larger the value of decay time is, the slower the decay speed and the better the afterglow properties are, and the smaller the phonon energy is. τ_1, τ_2, and τ_3 of $Ba_{0.14}Ga_2O_4:Cr_{0.06}$ are larger than those of $BaGa_2O_4:Cr_{0.06}$ and $BaGa_2O_4$, and the τ_{av} of $Ba_{0.14}Ga_2O_4:Cr_{0.06}$ was 1.13 times that of $BaGa_2O_4:Cr_{0.06}$ and 8.12 times that of $BaGa_2O_4$, which indicated that the optimized Cr^{3+}-doping and Ga:Ba ratio increased the number of the luminescence centers and the electron traps, respectively, resulting in a much longer PersL lifetime.

The NIR afterglow images (Figs. S1 and S2 in Supplementary Materials) of $BaGa_2O_4$, $BaGa_2O_4:Cr_{0.06}$, and $Ba_{0.14}Ga_2O_4:Cr_{0.06}$ indicated that the $BaGa_2O_4$ matrix exhibited excellent PersL properties after 2 days of excitation, indicating that there are appropriate number traps in BGO. The afterglow signal was still captured within 6 days (SNR = 11) after Cr^{3+} doping. Moreover, the SNR value was improved from 11 to 22 after changing the ratio of Ga:Ba. BGO and BGO:Cr can be repeatedly excited by the red LED lamp (665 ± 15 nm):

$$\tau_{av} = \frac{A_1\tau_1^2 + A_2\tau_2^2 + A_3\tau_3^2}{A_1\tau_1 + A_2\tau_2 + A_3\tau_3}. \quad (4)$$

3.2. Structure and particle analysis of BGO:Cr

Figure 3 shows the X-ray diffraction (XRD) patterns of the $BaGa_2O_4:Cr_x$ ($x = 0$, 0.006, 0.02, 0.04, 0.06, 0.08, and 0.10) PersL phosphors. All diffraction peaks of the $BaGa_2O_4:Cr_x$ PersL phosphors were consistent with those of the BGO planes crystal (PDF 46-0415), which indicated that the increase of Cr^{3+} contents did not influence the crystal structure of BGO.

There was only the diffraction peak of $BaGa_2O_4$ at 28.09° when a small amount of Ba existed in the crystal (Fig. S6 in Supplementary Materials), and other peaks were consistent with those of the β-Ga_2O_3 monoclinic structure. The intensity of the peak at 28.09° increased with the increase of the Ba content, and the Rietveld structure refinements of $Ba_{0.08}Ga_2O_4:Cr_{0.06}$ and $Ba_{0.14}Ga_2O_4:Cr_{0.06}$ indicate that the content of $BaGa_2O_4$ in the crystal will also increase (Fig. S7 in Supplementary Materials). Therefore, the $BaGa_2O_4:Cr_{0.06}$ PersL phosphor with pure $BaGa_2O_4$ phase was selected for further investigation.

The energy-dispersive X-ray spectroscopy (EDS) profiles of the $BaGa_2O_4:Cr_{0.06}$ PersL phosphor are shown in Fig. S8 of Supplementary Materials, indicating the presence of Ba, Ga,

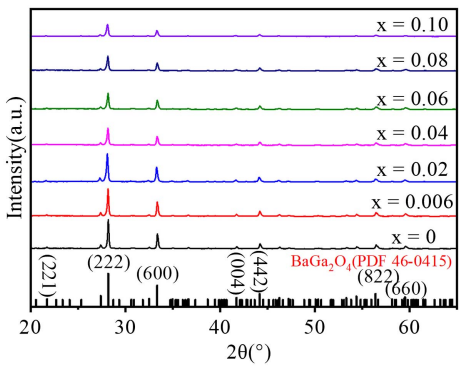

Fig. 3. XRD patterns of $BaGa_2O_4:Cr_x$ ($x = 0$, 0.006, 0.02, 0.04, 0.06, 0.08, and 0.10) PersL phosphors.

Cr, and O elements. The EDS mapping images showed that Ba, Ga, O, and Cr were homogeneously distributed in the phosphor particles (Fig. S9 in Supplementary Materials), suggesting the existence of Cr in the BGO host.

The $BaGa_2O_4:Cr_{0.06}$ PersL phosphor produced three excitation bands centered at 248 nm, 378 nm, and 512 nm at the emission wavelength of 753 nm (Fig. S3 in Supplementary Materials). The wavelengths at 378 nm and 512 nm belonged to the irregular transitions of $^4A_2(^4F) \rightarrow {}^4T_1(^4F)$ and $^4A_2(^4F) \rightarrow {}^4T_2(^4F)$ originated from Cr^{3+}. The strong band peak at 248 nm was attributed to the charge transfer of O-Cr[28]. These typical excitation bands also indicated that Cr^{3+} occupied the octahedral sites.

3.3. Mechanism of PersL of BGO:Cr

The thermoluminescence (TL) measurements were carried out and are portrayed in Fig. 4(a), which is with broadband ranging from 35°C to 225°C and a peak of 106°C. The half-width method was implemented to estimate the electron-trap-level depth of the $BaGa_2O_4:Cr_{0.06}$ PersL phosphor. The average electron-trap-level depth was deduced to be 0.619 eV[29], which showed that $BaGa_2O_4:Cr_{0.06}$ PersL phosphor was suitable for providing the PersL for a long time at room temperature[10]. There were many kinds of traps with different depths in the BGO:Cr PersL phosphor based on the width and peak temperature of the TL spectrum. The shallow traps were suitable for luminescence at room temperature, whereas the deep traps stored energy and prolonged the duration of the afterglow.

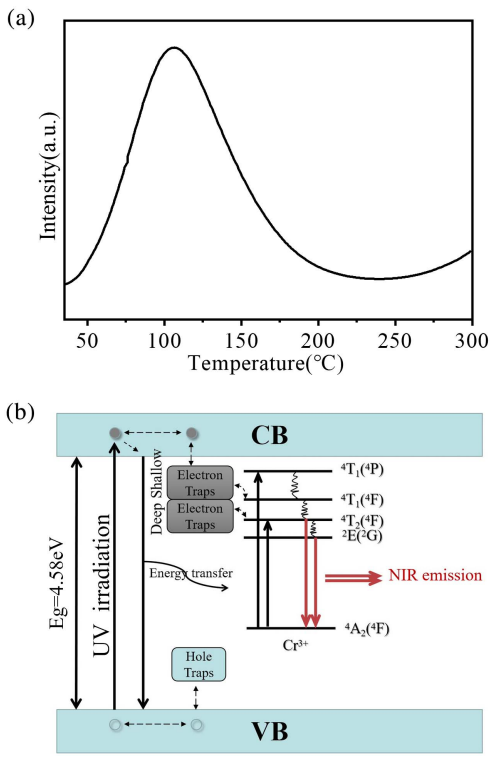

Fig. 4. (a) Thermoluminescence glow curve of $BaGa_2O_4:Cr_{0.06}$ PersL phosphor; (b) NIR PersL mechanism in the BGO:Cr PersL phosphors.

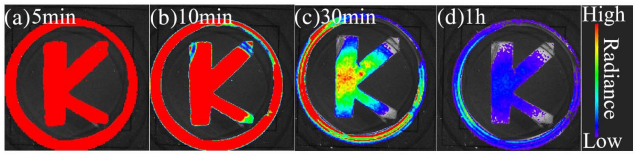

Fig. 5. Read-out (room temperature) pattern at (a) 5 min, (b) 10 min, (c) 30 min, and (d) 1 h after 254 nm UV light for 2 min.

Figure 4(b) shows the schematic energy diagram for demonstrating the PersL mechanism in the $BGO:Cr^{3+}$ PersL phosphor. The bandgap of un-doped BGO was 4.58 eV, corresponding to the host absorption. Under UV irradiation, the electrons were excited to the conduction band (CB), and the holes were spontaneously generated. At the same time, the excited electrons were captured into the natural defects of the BGO matrix by non-radiative relaxation. The absorbed energy was transmitted to Cr^{3+} ions via the host lattice, resulting in the $^4A_2(^4F) \rightarrow {}^4T_1(^4P)$, $^4A_2(^4F) \rightarrow {}^4T_1(^4F)$, and $^4A_2(^4F) \rightarrow {}^4T_2(^4F)$ transitions of Cr^{3+}. The $^2E(^2G) \rightarrow {}^4A_2(^4F)$ and $^4T_2(^4F) \rightarrow {}^4A_2(^4F)$ transitions of Cr^{3+} produced NIR emission. The excited electrons at $^4T_1(^4P)$ are captured by shallow electron traps through the CB and transferred to deep traps mainly via non-radiative relaxation[30]. After stopping the UV irradiation, PersL was produced by the recombination of the charge carriers and holes.

3.4. Information storage property of BGO:Cr

The potential application of BGO:Cr in information storage was tested. The information (the letter K) was first restored by the photo-mask-protected illumination of 254 nm light, and then the afterglows were captured. As shown in Fig. 5, $BaGa_2O_4:Cr_{0.06}$ displayed a fine shape at room temperature. These data further corroborated the existence of suitable traps in BGO:Cr at room temperature with excellent potential for information storage.

4. Conclusion

In conclusion, a novel NIR emitting wavelength-tunable BGO:Cr PersL phosphor was developed, and the application possibility of BGO:Cr phosphor in optical information storage was demonstrated. The developed BGO:Cr is expected to become a new medium for developing next-generation storage systems in the future.

Acknowledgement

The work was supported by the National Natural Science Foundation of China (NSFC) (No. 21867014) and Science and Technology Talents Training Project of Tianshan Youth Program of Xinjiang Uygur Autonomous Region (No. 2017Q086).

References

1. J. Hölsä, "Persistent luminescence beats the afterglow: 400 hundred years of persistent luminescence," Electrochem. Soc. Interface **18**, 42 (2009).
2. Z. J. Zhang, W. Li, N. Ma, and X. Y. Huang, "High-brightness red-emitting double-perovskite phosphor Sr_2LaTaO_6:Eu^{3+} with high color purity and thermal stability [Invited]," Chin. Opt. Lett. **19**, 030003 (2021).
3. Y. X. Zhuang, Y. Lv, L. Wang, W. W. Chen, T. L. Zhou, T. Takashi, H. Naoto, and R. J. Xie, "Trap depth engineering of $SrSi_2O_2N_2$: Ln^{2+},Ln^{3+}(Ln^{2+}=Yb, Eu; Ln^{3+}=Dy, Ho, Er) persistent luminescence materials for information storage applications," ACS Appl. Mater. Interfaces **10**, 1854 (2018).
4. B. Wang, Z. K. Chen, X. S. Li, J. C. Zhou, and Q. G. Zeng, "Photostimulated near-infrared persistent luminescence Cr^{3+}-doped Zn-Ga-Ge-O phosphor with high QE for optical information storage," J. Alloys Compd. **812**, 152119 (2020).
5. Y. Zhan, Y. Jin, H. Wu, L. Yuan, G. Ju, Y. Lv, and Y. Hu, "Cr^{3+}-doped $Mg_4Ga_4Ge_3O_{16}$ near-infrared phosphor membrane for optical information storage and recording," J. Alloys Compd. **777**, 991 (2019).
6. P. F. Smet, I. Moreels, Z. Hens, and D. Poelman, "Luminescence in sulfides: a rich history and a bright future," Materials **3**, 2834 (2010).
7. P. F. Smet, K. V. D. Eeckhout, and D. Poelman, "Persistent luminescence in non-Eu^{2+}-doped compounds: a review," Materials **6**, 2789 (2013).
8. V. Kahlenberg, R. X. Fischer, and J. B. Parise, "The stuffed framework structure of $BaGa_2O_4$," J. Solid State Chem. **154**, 612 (2000).
9. L. L. Noto, D. Poelman, V. R. Orante-Barrón, H. C. Swart, L. E. Mathevula, R. Nyenge, M. Chithambo, B. M. Mothudi, and M. S. Dhlamini, "Photoluminescence and thermoluminescence properties of $BaGa_2O_4$," Physica B **535**, 268 (2018).
10. H. F. Wang, X. Chen, F. Feng, X. Ji, and Y. Zhang, "EDTA etching: a simple way for regulating the traps, size and aqueous-dispersibility of Cr^{3+}-doped zinc gallate," Chem. Sci. **9**, 8923 (2018).
11. H. Li, J. Cai, R. Pang, G. Liu, S. Zhang, L. Jiang, D. Li, C. Li, J. Feng, and H. Zhang, "Strategy for developing thermal-quenching-resistant emitting and super-long persistent luminescence in $BaGa_2O_4$:Bi^{3+}," J. Mater. Chem. C **7**, 13088 (2019).
12. X. Q. Zhou, G. F. Ju, T. S. Dai, Y. Li, H. Y. Wu, Y. H. Jin, and Y. H. Hu, "Strontium substitution enhancing a novel Sm^{3+}-doped barium gallate phosphor with bright and red long persistent luminescence," J. Lumin. **218**, 116820 (2019).
13. A. Bessière, S. Jacquart, K. Priolkar, A. Lecointre, B. Viana, and D. Gourier, "$ZnGa_2O_4$:Cr^{3+}: a new red long-lasting phosphor with high brightness," Opt. Express **19**, 10131 (2011).
14. F. Liu, Y. J. Liang, and Z. W. Pan, "Detection of up-converted persistent luminescence in the near infrared emitted by the $Zn_3Ga_2GeO_8$:Cr^{3+}, Yb^{3+}, Er^{3+} phosphor," Phys. Rev. Lett. **113**, 177401 (2014).
15. O. Q. D. Clercq, L. I. D. J. Martin, K. Korthout, J. Kusakovskij, H. Vrielinck, and D. Poelman, "Probing the local structure of the near-infrared emitting persistent phosphor $LiGa_5O_8$:Cr^{3+}," J. Mater. Chem. C **5**, 10861 (2017).
16. N. Basavaraju, S. Sharma, A. Bessière, B. Viana, D. Gourier, and K. R. Priolkar, "Red persistent luminescence in $MgGa_2O_4$:Cr^{3+}: a new phosphor for *in vivo* imaging," J. Phys. D **46**, 375401 (2013).
17. J. Lee, P. W. Bisso, R. L. Srinivas, J. J. Kim, A. J. Swiston, and P. S. Doyle, "Universal process-inert encoding architecture for polymer microparticles," Nat. Mater. **13**, 524 (2014).
18. H. Lee, J. Kim, H. Kim, J. Kim, and S. Kwon, "Colour-barcoded magnetic microparticles for multiplexed bioassays," Nat. Mater. **9**, 745 (2010).
19. Y. Gao, B. N. Wang, L. Liu, and K. Shinozaki, "Near-infrared engineering for broad-band wavelength-tunable in biological window of NIR-II and -III: a solid solution phosphor of $Sr_{1-x}Ca_xTiO_3$:Ni^{2+}," J. Lumin. **238**, 118235 (2021).
20. M. Grinberg, P. I. Macfarlane, B. Henderson, and K. Holliday, "Inhomogeneous broadening of optical transitions dominated by low-symmetry crystal-field components in Cr^{3+}-doped gallogermanates," Phys. Rev. B **52**, 3917 (1995).
21. Y. Li, Y. Y. Li, R. C. Chen, K. Sharafudeen, S. F. Zhou, M. Gecevicius, H. H. Wang, G. P. Dong, Y. L. Wu, X. X. Qin, and J. R. Qiu, "Tailoring of the trap distribution and crystal field in Cr^{3+}-doped non-gallate phosphors with near-infrared long-persistence phosphorescence," Npg Asia Mater. **7**, e180 (2015).
22. T. A. Safeera, J. Johny, S. Shaji, Y. T. Nien, and E. I. Anila, "Impact of activator incorporation on red emitting rods of $ZnGa_2O_4$:Cr^{3+} phosphor," Mater. Sci. Eng. C **94**, 1037 (2019).
23. Y. X. Zhuang, J. Ueda, and S. Tanabe, "Enhancement of red persistent luminescence in Cr^{3+}-doped $ZnGa_2O_4$ phosphors by Bi_2O_3 codoping," Appl. Phys. Express **6**, 52602 (2013).
24. D. Q. Chen, Y. Chen, H. W. Lu, and Z. G. Ji, "A bifunctional Cr/Yb/Tm: $Ca_3Ga_2Ge_3O_{12}$ phosphor with near-infrared long-lasting phosphorescence and upconversion luminescence," Inorg. Chem. **53**, 8638 (2014).
25. X. M. Li, S. S. Zhou, R. F. Wei, X. Y. Liu, B. Q. Cao, and H. Guo, "Blue–green color-tunable emissions in novel transparent Sr_2LuF_7:Eu/Tb glass-ceramics for WLEDs," Chin. Opt. Lett. **18**, 051601 (2020).
26. C. G. Walsh, J. F. Donegan, T. J. Glynn, G. P. Morgan, G. F. Imbusch, and J. P. Remeika, "Luminescence from β-Ga_2O_3:Cr^{3+}," J. Lumin. **40**, 103 (1988).
27. M. D. Que, W. X. Que, T. Zhou, J. Y. Shao, and L. B. Kong, "Enhanced photoluminescence property of sulfate ions modified YAG:Ce^{3+} phosphor by co-precipitation method," J. Rare Earths **35**, 217 (2017).
28. J. S. Kim, J. S. Kim, and H. L. Park, "Optical and structural properties of nanosized $ZnGa_2O_4$:Cr^{3+} phosphor," Solid State Commun. **131**, 735 (2004).
29. Z. S. Liu, X. P. Jing, and L. X. Wang, "Luminescence of native defects in Zn_2GeO_4," J. Electrochem. Soc. **154**, H500 (2007).
30. Z. W. Pan, Y. Y. Lu, and F. Liu, "Sunlight-activated long-persistent luminescence in the near-infrared from Cr^{3+}-doped zinc gallogermanates," Nat. Mater. **11**, 58 (2012).